Resident and recruited macrophages differentially contribute to cardiac healing after myocardial ischemia

Tobias Weinberger[1,2,3,4], Denise Messerer[1,2], Markus Joppich[5], Max Fischer[1,2,3], Clarisabel Garcia[4], Konda Kumaraswami [1,2], Vanessa Wimmler[1,2], Sonja Ablinger[1,2], Saskia Räuber[1,2,6], Jiahui Fang[1,2], Lulu Liu[1,2], Wing Han Liu[1], Julia Winterhalter[1,2], Johannes Lichti[1], Lukas Tomas[1,2,3], Dena Esfandyari[3,7], Guelce Percin[8], Sandra Martin Salamanca[9], Andres Hidalgo[9,10], Claudia Waskow[8,11], Stefan Engelhardt[3,7], Andrei Todica[12], Ralf Zimmer[5], Clare Pridans[13,14], Elisa Gomez-Perdiguero[4], Christian Schulz[1,2,3]

[1]Medical Clinic I., Department of Cardiology, University Hospital, Ludwig Maximilian University, 81377 Munich, Germany

[2]Institute of Surgical Research at the Walter-Brendel-Centre of Experimental Medicine, University
Hospital, Ludwig Maximilian University, 81377 Munich, Germany

[3]DZHK (German Centre for Cardiovascular Research), partner site Munich Heart Alliance, 80336 Munich, Germany

[4]Institut Pasteur, Unité Macrophages et Développement de l'Immunité, Département de Biologie du Développement et Cellules Souches, Paris, France

[5]LFE Bioinformatik, Department of Informatics, Ludwig Maximilian University, 80333 Munich, Germany

[6]Department of Neurology, Medical Faculty, Heinrich Heine University of Düsseldorf, 40225 Düsseldorf, Germany

[7]Institute of Pharmacology and Toxicology, Technical University Munich, 80802 Munich,

24 Germany

25 [8]Immunology of Aging, Leibniz-Institute on Aging - Fritz-Lipmann-Institute (FLI), 07745 Jena,

26 Germany

27 [9]Area of Cell & Developmental Biology, Centro Nacional de Investigaciones Cardiovasculares

28 Carlos III, Madrid, Spain

29 [10]Vascular Biology and Therapeutics Program and Department of Immunobiology, Yale

30 University School of Medicine, New Haven, CT, USA

31 [11]Faculty of Biological Sciences, Friedrich-Schiller-University, 07737 Jena, Germany

32 [12]Department of Nuclear Medicine, Ludwig Maximilian University, 81377 Munich, Germany

33 [13]University of Edinburgh Centre for Inflammation Research, The Queen's Medical Research

34 Institute, Edinburgh EH16 4TJ, United Kingdom.

35 [14]Simons Initiative for the Developing Brain, Centre for Discovery Brain Sciences, University of

36 Edinburgh, Edinburgh EH8 9XD, United Kingdom

37

38 Corresponding author: Dr. Christian Schulz, MD

39 Address: Medical Clinic I., Department of Cardiology, University Hospital, Ludwig Maximilian

40 University, Marchioninistrasse 15, 81377 Munich, Germany

41 Phone: +49 89 440073092

42 Email: Christian.schulz@med.un-muenchen.de

43

44 ***Conflict-of-interest statement:*** The authors have declared that no conflict of interest exists.

ABSTRACT

Cardiac macrophages are heterogenous in phenotype and functions, which has been associated with differences in their ontogeny. Despite extensive research, our understanding of the precise role of different subsets of macrophages in ischemia/reperfusion injury remains incomplete. We here investigated macrophage lineages and ablated tissue macrophages in homeostasis and after I/R injury in a CSF1R-dependent manner. Genomic deletion of a fms-intronic regulatory element (FIRE) in the Csf1r locus resulted in specific absence of resident homeostatic and antigen-presenting macrophages, without affecting the recruitment of monocyte-derived macrophages to the infarcted heart. Specific absence of homeostatic, monocyte-independent macrophages altered the immune cell crosstalk in response to injury and induced proinflammatory neutrophil polarization, resulting in impaired cardiac remodelling without influencing infarct size. In contrast, continuous CSF1R inhibition led to depletion of both resident and recruited macrophage populations. This augmented adverse remodelling after I/R and led to an increased infarct size and deterioration of cardiac function. In summary, resident macrophages orchestrate inflammatory responses improving cardiac remodelling, while recruited macrophages determine infarct size after I/R injury. These findings attribute distinct beneficial effects to different macrophage populations in the context of myocardial infarction.

62 **GRAPHICAL ABSTRACT**

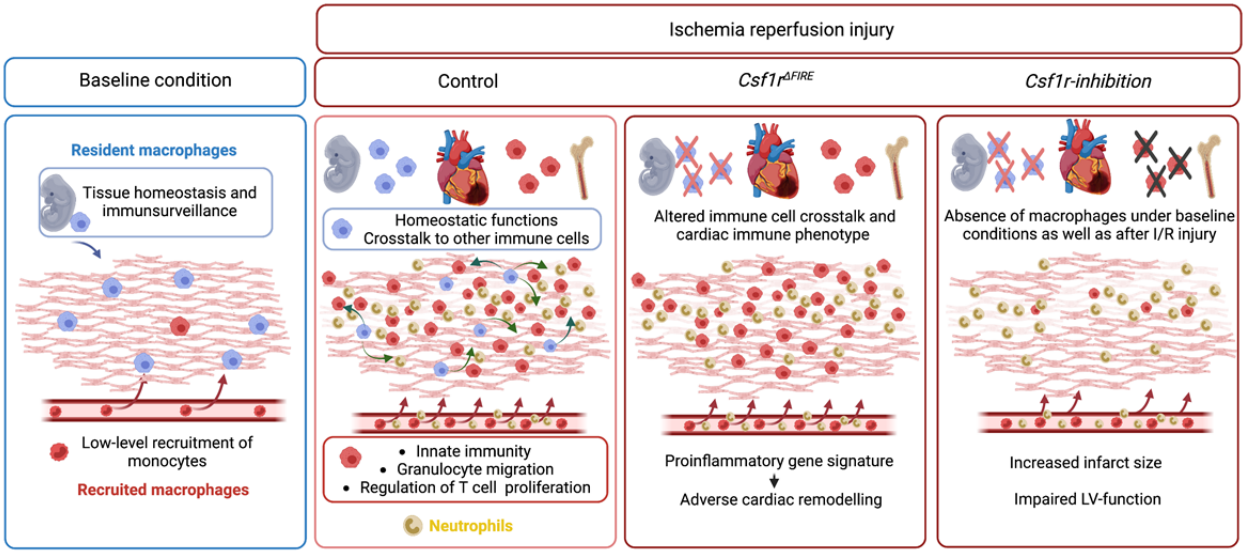

63

64

65 **INTRODUCTION**

66 Macrophages are important effectors of innate immunity. They are essential for host
67 defense against infections but are also involved in different cardiovascular diseases. They
68 represent the most abundant immune cell population in healthy cardiovascular tissues (Heidt *et*
69 *al*, 2014; Weinberger *et al*, 2020), where they contribute to organ functions (Hulsmans *et al*,
70 2017) and maintenance of tissue homeostasis (Nicolas-Avila *et al*, 2020). In cardiovascular
71 diseases such as atherosclerosis and its main sequelae, ischemic stroke and acute myocardial
72 infarction (AMI), macrophage functions are central to both disease development and healing.
73 AMI has remained a leading cause of mortality and morbidity worldwide (Ahmad & Anderson,
74 2021; Lozano *et al*, 2012). Although acute survival in this condition has improved through the
75 broad availability of percutaneous coronary intervention, adverse myocardial remodeling and
76 fibrosis frequently result in heart failure (Gerber *et al*, 2016). Pathophysiologically, the
77 diminished blood supply to myocardial tissue during AMI leads to acute tissue necrosis, which
78 induces a profound sterile inflammation and triggers complex cascade of immune processes and
79 tissue remodeling (Hilgendorf *et al*, 2014; Honold & Nahrendorf, 2018; Nahrendorf *et al*, 2007).
80 Consequently, uncontrolled immune reactions in the course of AMI are associated with impaired
81 wound healing and adverse remodeling and can result in worsened cardiac outcome (Panizzi *et*
82 *al*, 2010).

83 Macrophages play an essential role in cardiac injury, and thus represent a potential
84 therapeutic target (Hilgendorf *et al.*, 2014; Nahrendorf *et al.*, 2007). However, they are an
85 heterogeneous population (Kubota *et al*, 2019; Weinberger & Schulz, 2015; Zaman & Epelman,
86 2022), and a large body of work has shown that they can have both pro- and anti-inflammatory
87 functions. The differential roles of macrophage populations in AMI have remained incompletely

88 understood. Cardiac macrophages can derive from embryonic and adult hematopoietic
89 progenitors (Epelman *et al*, 2014). Fate mapping analyses have identified yolk sac (YS) erythro-
90 myeloid progenitors (EMPs) as a principal source of cardiac macrophages in adult life (Ginhoux
91 *et al*, 2010). However, limited labeling in inducible cre reporter systems have not allowed for
92 precisely differentiating and quantifying developmental origins of cardiac macrophages. Further,
93 targeting of these macrophages has been challenging (Frieler *et al*, 2015; Ruedl & Jung, 2018).

94 In this study, we investigated the cellular identity of cardiac macrophages in association
95 with their developmental paths and their immune responses to ischemia/reperfusion (I/R) injury.
96 By combining lineage tracing with single cell RNA sequencing, we provide an in-depth analysis
97 of the differential functions of resident and recruited cardiac macrophages. We then harnessed
98 mice with genomic deletion of the fms-intronic regulatory element (FIRE) (Rojo *et al*, 2019),
99 that allowed us to specifically address populations of resident macrophages in the infarcted heart
100 and compared them to mice, in which both recruited as well as resident macrophages are
101 depleted by pharmacological inhibtion of the CSF1R-signalling pathway. Using these
102 approaches of selective macrophage depletion, we could attribute different beneficial functions
103 to resident and also to recruited macrophages which impact differently on cardiac remodeling,
104 infarct size and cardiac outcome.
105

106 **RESULTS**

107 *Absence of resident cardiac macrophages in Csf1r$^{\Delta FIRE}$ mice*

108 To quantify the contribution of YS EMPs to cardiac resident macrophages, we harnessed
109 constitutive labeling in *Rank*^{Cre};*Rosa26*^{eYFP} mice (Jacome-Galarza *et al*, 2019; Mass *et al*, 2016;
110 Percin *et al*, 2018). ~80% of cardiac macrophages expressed YFP in hearts of 12 week-old
111 animals, whereas blood monocytes were not labeled (**Fig 1A; Fig EV1)**. EMP-derived microglia
112 served as control confirming high efficiency of Cre-mediated recombination. In a comparative
113 analysis, we traced fetal and adult definitive hematopoiesis in *Flt3*^{Cre}*Rosa26*^{eYFP} mice (Gomez
114 Perdiguero *et al*, 2015; Schulz *et al*, 2012), indicating that ~20% of cardiac macrophages derived
115 from definitive HSC **(Fig 1B)**. Thus, the majority of resident macrophages in the healthy heart is
116 of early embryonic origin.

117 To determine the role of resident macrophages in the mouse heart, we generated
118 *Rank*^{Cre}*Rosa26*^{DTR} mice that express the avian diphtheria toxin (DT) receptor in the EMP lineage,
119 rendering them susceptible to DT-mediated ablation. Administration of a single DT dose,
120 however, resulted in premature death of all mice (n=6) within 24 hours (**Fig EV2**). The injected
121 mice presented with a systemic inflammatory response syndrome (SIRS)-like phenotype,
122 indicating that acute depletion of EMP-derived macrophages is not viable.

123 In *Csf1r*$^{\Delta FIRE}$ mice, genetic deletion of the fms-intronic regulatory element (FIRE) in the first
124 intron of the *Csf1r* gene leads to a selective absence of tissue macrophages without the
125 developmental defects observed in *Csf1r*$^{-/-}$ mice (Munro *et al*, 2020; Rojo *et al.*, 2019). We first
126 confirmed that cardiac macrophages in *Csf1r*$^{\Delta FIRE/\Delta FIRE}$ *mice* (further termed ΔFIRE) mice were
127 reduced by ~90% and the number of monocytes and neutrophils was not altered **(Fig 1C-E)**. We
128 thus crossed the ΔFIRE animals with the YS EMP fate mapping line (*Rank*^{Cre}*Rosa26*^{eYFP} mice)

129 and showed that the macrophages absent in ΔFIRE animals were EMP-derived macrophages
130 **(Fig 1F)**, thus offering a new model to investigate the role of resident macrophages in cardiac
131 injury.

132 *Changes in the cardiac immune phenotype in Csf1r$^{\Delta FIRE}$ mice in baseline conditions*

133 To further characterize the macrophage populations absent in healthy hearts of adult ΔFIRE
134 mice, we carried out single cell RNA-sequencing (scRNA-seq) of CD45^{+} immune cells in
135 wildtype, ΔFIRE and *Rank^{Cre}Rosa26^{eYFP}* mice **(Fig 2A, Fig EV3)**. We identified the presence of
136 six macrophage clusters in control mice **(Fig 2B, Fig EV3)**. Two clusters of macrophages
137 expressing homeostatic (*e.g. Lyve-1, Gas6, Stab1*) and antigen presentation-related genes (*e.g.*
138 *CD74, H2-Ab1*) were specifically ablated in ΔFIRE mice **(Fig 2C)**, which largely represent YFP-
139 expressing macrophages in *Rank^{Cre}Rosa26^{eYFP}* mice **(Fig 2D).** Specifically, we mapped ~90% of
140 *yfp* transcripts to the two clusters of homeostatic and antigen presenting macrophages that were
141 ablated in ΔFIRE. Other clusters were not reduced in ΔFIRE, and also were not quantitatively
142 represented in the YS macrophage lineage tracing model, i.e. *Cx3cr1^{hi}* (2% *yfp*), *Ccr2^{low}Ly6c^{lo}*
143 (5% *yfp*) and *Ccr2^{hi}Ly6c^{hi}* (1% *yfp*) macrophages within respective clusters (**Fig 2D**). The
144 specific impact of ΔFIRE on resident macrophages is further supported by the observation, that
145 no changes in gene expression nor cell numbers were observed in *Ly6c^{hi}* monocytes and
146 inflammatory *Ccr2^{hi}Ly6c^{hi}* macrophages **(Fig 2C Fig EV4)**. Together, ΔFIRE allows for
147 investigating the role of resident cardiac macrophages that are largely of YS origin.

148 Absence of resident macrophages in ΔFIRE was associated with changes in gene expression in
149 non-macrophage clusters such as *T- and B-cells* and *natural killer (NK)* cells (**Fig EV5**). Further,
150 overall phagocytic capacity, as inferred by expression of phagocytosis related genes (Amorim *et*

151 *al*, 2022), was reduced (**Fig 2E**). This suggests that absence of resident macrophages is
152 accompanied by distinct changes in immune functions in the homeostatic heart.

153 *Adverse cardiac remodeling in Csf1r$^{\Delta FIRE}$ mice after I/R injury*

154 To assess the impact of the absence of resident macrophages in cardiac injury, we
155 subjected ΔFIRE mice to I/R injury and investigated remodeling and functional outcome by
156 sequential positron emission tomography (PET) imaging after 6 and 30 days **(Fig 3A)**. Function
157 of the cardiac left ventricle (LV), as determined by ejection fraction (LVEF) and stroke volume
158 (SV), improved in controls in the course of post-I/R remodeling **(Fig 3B-C)**. In contrast, LVEF
159 and SV remained unchanged or worsened in ΔFIRE mice, and longitudinal observations of mice
160 indicated a negative net effect on ejection fraction from day 6 to day 30 post I/R. Thus, absence
161 of resident macrophages had a negative effect on cardiac remodeling **(Fig 3D-G)**. Nonetheless,
162 infarct size as determined by viability defect (PET) and fibrotic area (histology) was not different
163 after 30 days **(Fig 3E-H)**.

164 *Recruitment of BM-derived macrophages into infarct zone of Csf1r$^{\Delta FIRE}$ mice*

165 To gain a deeper understanding of the inflammatory processes taking place in the
166 infarcted heart, we quantified macrophage distribution by immunofluorescence and flow
167 cytometry analysis of ischemic and remote areas after I/R. In ΔFIRE mice, macrophages were
168 largely absent in the remote zone of infarcted hearts **(Fig 4A)**, indicating sustained depletion of
169 resident macrophages. However, macrophages strongly increased in the infarct area and their
170 numbers were not different in both infarct and border zones between ΔFIRE and control mice
171 **(Fig 4A)**. This indicated recruitment and differentiation of ΔFIRE-independent macrophages
172 from the circulation into these regions. Indeed, complementing lineage tracing of BM HSC in
173 *Flt3^{Cre}* mice (**Fig 4B**) and YS EMP in *Rank^{Cre}* mice (**Fig 4C**) proved the recruitment of

174 macrophages from BM HSC (Flt3 GFP+ and Rank RFP-, respectively) in the early phase of I/R
175 injury. 30 days after I/R, BM-derived macrophages remained overrepresented in the infarct zone
176 (~75% HSC contribution), and differential contribution of BM HSC declined from the border
177 zone (~50%) to the remote zone (~35%) **(Fig 4D)**. Taken together, recruited BM-derived
178 macrophages represent the main population in the infarct area and their recruitment was
179 unaltered in ΔFIRE mice. This supports the notion that resident macrophages influence cardiac
180 remodeling but recruited macrophages drive infarct size after I/R.

181 *Transcriptional landscape of resident versus recruited macrophages in I/R injury*

182 To address the differential responses of resident and recruited macrophages to I/R injury, we
183 generated BM chimeric mice. We applied an irradiation-independent model using conditional
184 deletion of c-myb to deplete BM hematopoietic cells in CD45.2 mice and replace them with
185 CD45.1 donor HSC. 2 days after I/R injury, we FACS-sorted recruited ($CD45.1^+$) and resident
186 ($CD45.2^+$) macrophages and carried out bulk RNA sequencing **(Fig 5A)**. The two macrophage
187 populations exhibited profound transcriptional differences after I/R injury. Expression of
188 homeostasis-related genes like *Timd4, Lyve-1, CD163* and *Retnla* was increased in resident
189 $CD45.2^+$ macrophages **(Fig 5B, C).** Substantiating the differential regulation of macrophage
190 programs, $CD45.1^+$ macrophages increased inflammatory- and host defense-related gene
191 ontology (GO) terms (e.g. myeloid leukocyte related immunity, killing of cells), whereas
192 $CD45.2^+$ macrophages upregulated development- and homeostasis-related GO terms (e.g.
193 extracellular matrix organization, vasculature development, heart muscle development) **(Fig 5D)**.
194 GO enrichment analysis further predicted that processes involved in innate (e.g. leukocyte
195 migration, regulation of defense response, response to bacterium) as well as the adaptive
196 immunity (e.g. T cell selection, T cell activation, B cell proliferation) were increased in $CD45.1^+$

197 macrophages after infarction **(Fig 5D)**. Thus, resident and recruited macrophages provide distinct
198 transcriptional changes and inferred functions in response to I/R.

199 *Altered inflammatory patterns and immune cell communication in Csf1r$^{\Delta FIRE}$ mice*

200 To evaluate the immune response of resident and recruited macrophages to I/R injury in ΔFIRE
201 mice, we interrogated the transcription profile of CD45^{+} cells from the infarct area **(Fig 6A)**. In
202 contrast to the absence of homeostatic and antigen-presenting macrophage clusters in healthy
203 hearts of ΔFIRE mice **(Fig 2B-C)**, there were less differences in immune cell clusters between
204 ΔFIRE and control mice 2 days after I/R **(Fig 6B, C)**. Abundance of homeostatic macrophages
205 was also reduced at this time point, however, other clusters including *Ccr2^{hi}Ly6c^{hi}* inflammatory
206 macrophages were not altered, which is in line with our histological findings.

207 ΔFIRE was associated with some changes in gene expression in cardiac non-macrophage
208 immune cells. Across different clusters, including lymphocyte and neutrophil clusters,
209 expression of anti-inflammatory genes like *Chil3 (Ym1)* and *Lcn2* was reduced**.** Vice versa,
210 expression of Bcl-family genes like *Blc2a1a* and *Bcl2a1d*, which are associated with apoptosis
211 and inflammatory pathways, was higher in ΔFIRE mice **(Fig EV6-8)**. Other upregulated genes
212 were related to antigen presentation (e.g.*CD74, H2-Ab1*), as identified in the *Ccr2^{lo}Ly6c^{lo},*
213 homeostatic and *Ccr2^{hi}Ly6c^{hi}* macrophage clusters **(Fig EV6 and 7)**. Further, we interrogated
214 inflammatory gene expression in neutrophils, which are abundant first responders to myocardial
215 infarction. We found that a computed score summing up inflammasome activation (Amorim *et*
216 *al.*, 2022) was increased in all neutrophil clusters in ΔFIRE mice (**Fig 6D**). Thus, the absence of
217 cardiac macrophages was associated with altered inflammatory properties of non-macrophage
218 immune cells in the infarcted heart.

219 Altered intercellular crosstalk of macrophages is a hallmark of cardiac inflammation. We
220 therefore assessed ligand-receptor (LR) interactions between immune cell populations after I/R
221 injury. Indeed, the number of LR interactions with neutrophils and lymphocytes, as well as the
222 strength of the macrophage-emitted communication signals was markedly reduced in
223 homeostatic, antigen-presenting and *Ccr2^{lo}Ly6c^{lo} Mø* macrophage clusters (**Fig 6E, F)**. In
224 contrast, immune cell communication in BM-derived macrophage clusters (e.g. *Ccr2^{hi}Ly6c^{hi} Mø*
225 *cluster,* **Fig EV9***)* was not different to control mice. Taken together, deficiency in resident
226 macrophages in I/R injury altered the intercellular immune crosstalk and induced a pro-
227 inflammatory signature in e.g. cardiac neutrophils. However, transcriptional profiles of BM-
228 derived inflammatory macrophages were largely unaltered. Together with our histological
229 analysis showing the dominance of recruited BM-derived macrophages in the early phase of I/R,
230 this potentially explained the limited impact of ΔFIRE on functional outcome after I/R injury.

231

232 *Ablation of resident and recruited macrophages severely impacts on cardiac healing after I/R*
233 *injury*

234 To test this hypothesis, we determined the effect of combined ablation of resident and recruited
235 macrophages. We therefore exposed mice to continuous treatment with the CSF1R-inhibitor
236 PLX5622 (**Fig 7A**). In healthy hearts, inhibitor treatment resulted in the absence of cardiac
237 macrophages within 3 days, which had no impact on cardiac function (**Fig EV10**). We then
238 subjected mice to I/R injury and investigated outcome by sequential PET imaging and histology
239 **(Fig 7A)**. Treatment with PLX5622 diminished macrophage numbers in both remote and infarct
240 areas in the early phase (day 2) after injury. Recruitment of other myeloid cells e.g. neutrophils
241 was not altered in this context (**Fig 7B**). This effect was pronounced in the chronic phase (day

242 30) after I/R injury, in which macrophages were largely absent in remote, border and infarct
243 zones (**Fig 7C,D**). Absence of resident and recruited macrophages was associated increased
244 infarct size, as determined by fibrosis area (WGA histology) as well as viability defect (PET),
245 and resulted in deterioration of cardiac function **(Fig 7E-I).** Specifically, LVEF was reduced 6
246 days after I/R, and remained strongly impaired at 30 days **(Fig 7E).**

247 Taken together, sole absence of resident macrophages had limited negative impact on cardiac
248 remodeling. Absence of both resident and recruited macrophages resulted in a significant
249 increase in infarct size and deterioration of left ventricular function after I/R injury, highlighting
250 a beneficial effect of recruited macrophages in cardiac healing.
251

252 **DISCUSSION**

253 Macrophages are key players in cardiac homeostasis and disease (Bajpai *et al*, 2019;
254 Bajpai *et al*, 2018; Dick *et al*, 2019; Epelman *et al.*, 2014; Hulsmans *et al.*, 2017; Nahrendorf *et*
255 *al.*, 2007; Nicolas-Avila *et al.*, 2020; Panizzi *et al.*, 2010; Sager *et al*, 2016). The precise
256 understanding of their developmental origin, their functions and their regulation could enable the
257 identification of macrophage-targeted strategies to modify inflammation in the heart. This study
258 sheds light on the differential role of resident and recruited macrophages in cardiac remodeling
259 and outcome after AMI.

260 BM-derived recruited macrophages are a scarce population in the healthy heart but are
261 recruited in vast numbers to the injured myocardium after I/R injury. These recruited cells
262 exhibit substantially different transcriptional profiles in comparison to their resident counterpart,
263 and show pro-inflammatory properties. Resident macrophages remain present in the remote and
264 border zone and display a reparative gene expression profile after I/R injury. In comparison to
265 recruited macrophages, resident macrophages expressed higher levels of genes related to
266 homeostatic functions (e.g. *Lyve-1, Timd4, CD163, Stab1*). These markers have recently been
267 associated with self-renewing tissue macrophages that are maintained independently of BM
268 contribution (Dick *et al*, 2022). Biological processes associated with cardiac healing are
269 upregulated in resident macrophages (e.g. regulation of vascular development, regulation of
270 cardiomyocyte development, extracellular matrix organization). Transcriptional profiles of
271 recruited macrophages show enhanced inflammatory biological processes also in macrophages
272 harvested from the remote area, underlining their potentially detrimental influence on remote
273 cardiac injury.

274 Two recent studies addressed the role of resident macrophages using DT-mediated
275 macrophage depletion and reported impaired cardiac remodeling in chronic myocardial
276 infarction (Dick *et al.*, 2019) and after I/R injury (Bajpai *et al.*, 2019). However, DT-mediated
277 cell ablation is known to induce neutrophil recruitment and tissue inflammation (Frieler *et al.*,
278 2015; Oh *et al*, 2017; Ruedl & Jung, 2018; Sivakumaran *et al*, 2016). This inflammatory
279 preconditioning of cardiac tissue after DT-depletion is likely to impact on cardiac remodeling
280 and influence assessment of tissue macrophage functions. Genomic deletion of FIRE in the *Csf1r*
281 gene results in the near-absence of resident cardiac macrophages but circumvents the
282 inflammatory stimulus of DT-induced depletion. ΔFIRE specifically diminished homeostatic and
283 antigen-presenting macrophages. Substantiating the specificity to resident cardiac macrophages
284 in this genetic model, the amount of macrophages recruited to the infarct area after I/R injury
285 was not affected in ΔFIRE mice. Further, scRNAseq analysis revealed that gene expression of
286 monocytes as well as *Ccr2*^{hi}*Ly6c*^{hi} *and Cx3cr1*^{hi} Mϕ, representing mainly recruited immune
287 cells, was mostly unchanged in ΔFIRE compared to control mice. The specific targeting of the
288 resident macrophage population introduces an interesting in vivo model for studying their role in
289 MI without the need for inflammation-prone conditional deletion of macrophages (Frieler *et al.*,
290 2015).

291 Ablation of resident macrophages altered macrophage crosstalk to non-macrophage
292 immune cells, especially lymphocytes and neutrophils. This was paralleled by a proinflammatory
293 gene signature in neutrophils, with increased expression of inflammasome-related genes and a
294 reduction in anti-inflammatory genes like *Chil3* and *Lcn2* (Gordon & Martinez, 2010; Guo *et al*,
295 2014; Parmar *et al*, 2018). Interestingly, inflammatory polarization of neutrophils is associated
296 with poor outcome also after ischemic brain injury (Cuartero *et al*, 2013). Consequently, absence

297 of resident macrophages worsened cardiac remodeling in the late postinfarction phase in ΔFIRE
298 mice indicating their biological role in myocardial healing. However, absence of resident
299 macrophages did not change infarct size or impact on LV function.

300 Depletion of macrophages by pharmacological inhibition of CSF1R induced the absence
301 of both resident and recruited macrophages, allowing us to determine cardiac outcome in
302 juxtaposition to the ΔFIRE mice. Continuous CSF1R inhibition induced the absence of
303 macrophages also in the infarcted area and had deleterious effect on infarct size and LV function.
304 In line with our findings, depletion of macrophages by anti-CSF1R treatment was associated
305 with worsened cardiac function in a model of pressure overload induced heart failure (Revelo *et*
306 *al*, 2021). Controversially, a recent study in which monocytes were depleted using DT-injections
307 in *Ccr2*^{DTR} mice reported beneficial effects on cardiac outcome after MI in mice. However, other
308 immune cells including neutrophils express CCR2 and may therefore be affected directly (Talbot
309 *et al*, 2015; Xu *et al*, 2017). In line with this, Ccr2-deficient mice exhibit reduced acute
310 recruitment of neutrophils to the brain after I/R injury, which was associated with reduced infarct
311 size and brain edema (Dimitrijevic *et al*, 2007).

312 Taken together our study underlines the heterogeneity of cardiac macrophages and the
313 importance of ontogeny therein. Resident macrophages, which mainly derive from YS EMPs,
314 govern cardiac homeostasis in the healthy heart, and contribute positively to cardiac healing after
315 I/R injury by orchestrating anti-inflammatory programming of other cardiac immune cells.
316 However, recruited macrophages contribute to the healing phase after AMI and their absence
317 defines infarct size and cardiac outcome.

318

319

320 **MATERIALS AND METHODS**

321 *Mice*

322 *Rank*^{Cre} (Jacome-Galarza *et al.*, 2019; Percin *et al.*, 2018), *Flt3*^{Cre} (Benz *et al*, 2008),
323 *Myb*$^{fl/fl}$ (Emambokus *et al*, 2003), *Mx1*^{Cre} (Kuhn *et al*, 1995) (from The Jackson Laboratory
324 (JAX), Stock No: 003556), *Csf1r*$^{\Delta FIRE}$ (Rojo *et al.*, 2019), *Rosa26*^{DTR} (Buch *et al*, 2005) (JAX
325 Stock No: 007900), *Rosa26*$^{mT/mG}$ (Muzumdar *et al*, 2007) (JAX Stock No: 007676), *Rosa26*^{eYFP}
326 (Srinivas *et al*, 2001) (JAX Stock No: 006148), and *Rosa26*^{RFP} (JAX Stock No: 034720) mice have been
327 previously described. PCR genotyping was performed according to protocols described
328 previously. Animals were aged between 10-16 weeks. We have complied with all relevant
329 ethical regulations. Animal studies were approved by the local regulatory agency (Regierung von
330 Oberbayern, Munich, Germany, record numbers ROB-55.2-2532.Vet_02-19-17 and ROB-55.2-
331 2532.Vet_02-19-1; Care and Use Committee of the Institut Pasteur (CETEA), dap190119).

332 For fate-mapping analysis of Flt3^{+} precursors, *Flt3*^{Cre} males (the transgene is located on
333 the Y chromosome) were crossed to *Rosa26*^{eYFP} or *Rosa26*$^{mT/mG}$ female reporter mice and only
334 the male progeny was used. For all other experiments, the offspring of both sexes was used for
335 experiments.

336 BM transplantation was enabled by conditional deletion of the transcription factor *myb* as
337 previously described (Stremmel *et al*, 2018). In brief, we induced BM ablation by 4 injections of
338 polyI:C into *CD45.2; Mx1*^{Cre}*Myb*$^{flox/flox}$ every other day, and then transplanted BM from congenic
339 *C57BL/6 CD45.1* (*Ly5.1*; JAX Stock No: 006584). We confirmed the success (chimerism of
340 above 90%) of the BM-transplantation after 4 weeks**.**

341 To deplete macrophages, we used the selective CSF1R-inhibitor PLX5622. Control and
342 PLX5622 (300 ppm formulated in AIN-76A standard chow, Research Diets, Inc.) chows were
343 kindly provided by Plexxikon Inc (Berkeley, CA). For depletion of RANK-lineage macrophages,
344 *Rank*^{Cre}*Rosa26*^{DTR} mice were injected intraperitoneally with 0.02 mg/kg body weight diphtheria
345 toxin (DT; Sigma-Aldrich) at the timepoints mentioned in Fig ure and corresponding legend.
346 Mice were closely monitored by veterinarians and according to score sheets that were approved
347 by the regulatory agency. Single DT application in *Rank*^{Cre}*Rosa26*^{DTR} mice let to rapid
348 deterioration of their health (without infarction or other interventions), and consequently
349 experiments needed to be aborted according to regulations; experimental outcomes were then
350 documented as premature death as indicated.

351 *Ischemia-reperfusion (I/R) injury*

352 I/R injury was carried out as previously described (Nicolas-Avila *et al.*, 2020). In brief,
353 mice were anesthetized using 2% isoflurane and intraperitoneal injection of fentanyl (0.05
354 mg/kg), midazolam (5.0 mg/kg) and medetomidine (0.5 mg/kg), and then intubated orally
355 (MiniVent Ventilator model nr. 845, Harvard Apparatus®) and ventilated (volume of 150 µL at
356 200/min). After lateral thoracotomy, the left anterior descending artery (LAD) was ligated with
357 an 8-0 prolene suture producing an ischemic area in the apical left ventricle (LV). To induce the
358 reperfusion injury, the suture was removed after 60 min and reperfusion was confirmed by
359 observing the recoloring of the LV. For experiments with CD169-DTR mice, animals were
360 anesthetized with xylazine and ketamine, and duration of ischemia was 45 min in the I/R model
361 as described earlier (Nicolas-Avila *et al.*, 2020). Postoperative analgesia was performed by
362 injection of Buprenorphin (0.1 mg/kg) twice per day for 3 days. After 2, 6 or 30 days after I/R
363 injury organs were harvested after cervical dislocation.

364 *Organ harvest*

365 Mice were anaesthetized using 2% isoflurane and organ harvest was performed after
366 cervical dislocation. Blood was harvested with a heparinized syringe (2mL) by cardiac puncture.
367 After perfusion with 20 mL of ice-cold PBS hearts were excised and kept in PBS on ice until
368 further tissue processing. For flow cytometry, hearts were divided into the ischemia (tissue distal
369 of the LAD ligation) and remote area (tissue proximal of the LAD ligation). For histological
370 examinations of tissues, hearts were incubated in 4% PFA for 30 min followed by an incubation
371 in 30% sucrose-solution (Sigma Aldrich®) for 24 h. Afterwards, hearts were mounted onto a
372 heart slicing device and cut transversally into 3 equal parts (termed level 1, 2 and 3) and stored in
373 Tissue-Tek® (Sakura Finetek Germany GmbH) at -80°C.

374 *Immunohistology*

375 Cryosections (10-12 µm) of heart tissue were fixed with 4% paraformaldehyde for 10
376 min. Blocking and permeabilization were performed with 0.5% Saponin and 10% goat serum for
377 1h. Primary antibodies were added and incubated for 2-18 h (see Supplemental Table 1). Slides
378 were washed with PBS and secondary antibodies were added and incubated for 1h (see
379 Supplemental Table 1). WGA-staining (Wheat Germ Agglutinin Alexa Fluor™ 647 conjugated
380 antibody, ThermoFisher Scientific®) was used to locate and measure the infarct area and nuclei
381 were stained with DAPI. Finally, slides were washed one more time and Fluorescence Mounting
382 Medium was used to cover the stained sample.

383 Heart samples were evaluated using an Axio Imager M2 (Carl Zeiss®) and blinded
384 picture analysis was performed using ZEN Imaging and Axiovision SE64 Rel. 4.9.1 (Carl
385 Zeiss®). For the evaluation of cell numbers, 6 individual high-resolution images from each
386 respective anatomical region (infarct area, border zone and remote zone) were analysed for each

387 animal. To measure infarct size the heart was cut into 3 parts and the infarcted area was
388 measured as WGA^+ area in sections from each part.

389 *Flow cytometry*

390 100 µL of heparinized blood was used for FACS analysis. Erythrocytes were lysed with
391 1% ammonium chloride. After washing with PBS, the cell suspension was resuspended in
392 purified rat anti-mouse CD16/CD32 (BD Pharmingen®) and incubated for 15 min at 4°C.
393 Following this, cells were incubated with FACS-antibodies for 15 min at 4°C **(table S1)**.

394 Heart tissue was dissected into remote and ischemic tissue as described above and
395 minced into small pieces using forceps and a scalpel. When comparing baseline and I/R injury in
396 FACS analysis, basal heart tissue was used for comparison with remote tissue and apical heart
397 tissue for comparison with ischemia tissue. After enzymatic digestion (Collagenase XI 1200
398 U/mg, Collagenase I 125 U/mg, Hyaluronidase 500 U/mg, DNase I 1836 U/mg; Sigma
399 Aldrich®) for 30 min at 37°C cells were washed and incubated with purified anti-CD16/32
400 (FcγRIII/II; dilution 1/50) for 10 min. Thereafter, cells were incubated wit FACS-antibodies
401 (**table S1**) for 30 min at 4°C. FACS-analysis was performed on a BD Fortessa® or a
402 BeckmanCoulter Cytoflex® flow cytometer and gating strategies are shown in Supplemental Fig
403 ures 1 and 3. Data were analysed using FlowJo® (version 10.0.8r1).

404 *Cell Sorting*

405 Cell sorting was performed on a MoFlo Astrios (Beckman Coulter) to obtain cardiac
406 macrophages from *CD45.2; Mx1*^{Cre}*Myb*$^{flox/flox}$ after BM-transplantation of CD45.1 BM (n=3 for 2
407 days after I/R injury) for bulk sequencing, or all cardiac immune cells ($CD45^+$ cells) of
408 *Csf1r*$^{\Delta FIRE}$ and *Rank*^{Cre}*Rosa26*^{eYFP} mice (n=3 for *Csf1r*$^{\Delta FIRE/+}$ and *Csf1r*$^{\Delta FIRE/\Delta FIRE}$ in baseline

409 conditions, n=1 for *Rank*^{Cre}*Rosa26*^{eYFP} in baseline conditions; n=2 for *Csf1r*$^{\Delta FIRE/+}$ and
410 *Csf1r*$^{\Delta FIRE/\Delta FIRE}$ 2 days after I/R injury) for single cell analysis. CD45^{+} cells were enriched by
411 using magnetic beads and MS columns (CD45 MicroBeads; Miltenyi Biotec). Cells were then
412 sorted as single/live/CD45^{+} cells for single cell sequencing from baseline hearts and from the
413 ischemic myocardium 2 days after I/R injury. Bulk sequencing was performed on
414 single/live/CD45^{+}/lin^{-}/CD11b^{+}/F4/80^{+}/CD64^{+}/CD45.1^{+} or CD45.2^{+} cells from the remote and the
415 ischemic myocardium 2 days after I/R injury. Dead cells were identified with SYTOX Orange
416 Dead Cell Stain.

417 *Bulk sequencing and analysis*

418 For each sample, ~1000 macrophages were sorted into 75µL of RLT buffer (Qiagen,
419 containing 1% beta-mercaptoethanol), vortexed for 1 min and immediately frozen (-80°C). RNA
420 extraction (RNeasy® Plus Micro Kit, Qiagen), cDNA generation (SMART®-Seq v4 Ultra Low
421 Input RNA Kit, Takara Bio) and library preparation (Nextera® XT DNA Library Prep Kit,
422 Illumina) were performed according to the manufacturer's specifications. Sequencing was
423 performed on a HiSeq4000 system (Ilumina).

424 The obtained reads were trimmed using bbduk from the BBMap
425 (https://sourceforge.net/projects/bbmap/) v38.87 collection using parameters "ktrim=r k=23
426 mink=11 hdist=1 tpe tbo". The trimmed reads were aligned with Hisat2 2.2.1 against the
427 Ensembl release 102 reference mouse genome (Yates *et al*, 2020).

428 Gene expression was quantified using the featureCounts (Liao *et al*, 2014) application
429 from the subread package (v2.0.1) and with parameters "--primary -O -C -B -p -T 8 --
430 minOverlap 5". Differential expression analysis was performed using DESeq2 (v1.30.0) (Love *et*
431 *al*, 2014). A Gene Ontology Set Enrichment analysis was performed using the ClusterProfiler R

432 package (v3.18.1). The visualization of the respective clustermaps was layouted using the
433 ForceAtlas2 implementation of the python fa2 (https://pypi.org/project/fa2/) package for
434 networkx (v2.5) (https://networkx.org/).

435 On the library-size normalized count data, the pymRMR ((Peng *et al*, 2005),
436 https://pypi.org/project/pymrmr/) package was used to derive the top 100 discriminatory genes
437 (Mutual Information Quotient method) for subsequently calculating the UMAP 2D-embedding (
438 (McInnes *et al*, 2020), (https://pypi.org/project/umap-learn/)) for all samples (umap-learn
439 package v0.5.0rc1, 3 neighbors) ((McInnes *et al*, 2018), https://pypi.org/project/pymrmr/).

440 *Single cell RNA sequencing and analysis*

441 After sorting, cells were proceeded for single cell capture, barcoding and library
442 preparation using Chromium Next GEM single cell 3' (v3.1, 10x Genomics) according to
443 manufacturer's specifications. Pooled libraries were sequenced on an Illumina HiSeq1500
444 sequencer (Illumina, San Diego, USA) in paired-end mode with asymmetric read length of
445 28+91 bp and a single indexing read of 8bp.

446 The reads of heart1 sample ($Rank^{Cre}Rosa26^{eYFP}$) were demultiplexed using Je-
447 demultiplex-illu (Girardot *et al*, 2016) and mapped against a customized mouse reference
448 genome (GRCm38.p6, Gencode annotation M24) including eYfp sequence using CellRanger
449 (v3.1.0, 10x Genomics).

450 The six mouse samples 20133-0001 to 20133-0006 (baseline condition of $Csf1r^{\Delta FIRE/+}$
451 and $Csf1r^{\Delta FIRE/\Delta FIRE}$), were processed using Cellranger 4.0.0 using the 2020A mm10 reference.

452 The 4 mouse samples (MUC13956-13959, infarct condition of $Csf1r^{\Delta FIRE/+}$ and
453 $Csf1r^{\Delta FIRE/\Delta FIRE}$), were sequenced with 4 technical sequencing replicates and pooled using the

454 cellranger (v4.0.0, 10x Genomics) pipeline. Cellranger 4.0.0 was called with default parameters
455 and the 2020A mm10 reference for gene expression.

456 Finally, all 11 samples were integrated using Seurat 4.0.0 (on R 4.0.1) (Stuart & Satija,
457 2019). The samples were processed, and cells were filtered to contain between 200 and 6000
458 features, have at least 1000 molecules detected (nCount_RNA > 1000), have below 15% mtRNA
459 content (^MT) and below 40% ribosomal RNA content (^Rps|^Rpl). After this filtering a total of
460 35759 cells remained.

461 After performing SCTransform (Hafemeister & Satija, 2019) on the samples, the SCTransform
462 vignette for integrating the datasets was followed (with 2000 integration features). For
463 dimensionality reduction, PCA was performed using default parameters, and UMAP and
464 Neighbour-Finding was run on 50 PCs. Clustering was performed at a resolution of 0.8. A total
465 of 18 clusters was identified using this approach. Cluster markers were calculated using the t-test
466 in the FindMarkers function. Subsequently cell types were initially predicted using the cPred cell
467 type prediction (https://github.com/mjoppich/scrnaseq_celltype_prediction). Upon manual
468 curation, further fine-grained cell type annotations were made. Differential comparisons were
469 performed against several subgroups of the data set. These comparisons were performed using
470 the t-test in the FindMarkers function of Seurat. Differential results are visualized using the
471 EnhancedVolcano library (Blighe K, 2021).

472 For the analysis of cell-cell interactions we downloaded the ligand-receptor pairs from Jin
473 et al. (Jin *et al*, 2021) from the Lewis Lab GitHub repository
474 (https://github.com/LewisLabUCSD/Ligand-Receptor-Pairs). For each interaction (ligand-
475 receptor pair for a cluster-pair) the communication score is calculated as the expression product
476 (Armingol *et al*, 2021) of the mean normalized expressions exported from the Seurat object. This

477 ensures that little expression of either ligand or receptor in only one cluster results in a relatively
478 low communication score, and only good expression of ligand and receptor will result in a high
479 communication score. The direction of an interaction is fixed from ligand to receptor. The single
480 ligand-receptor-communication-scores were then aggregated (sum) such that only interactions
481 with a score greater six were taken into account.

482 Gene module scores for inflammasome, ROS and phagocytosis gene sets were calculated
483 using Seurat's AddModuleScore function. All scripts, including the ones for creating the
484 visualizations of bulk and scRNA-seq data, are available online through
485 https://github.com/mjoppich/myocardial_infarction .

486 *In Vivo PET Imaging*

487 ECG-gated positron emission tomography (PET) images were performed on day 6 and 30
488 after I/R injury of the LAD using a dedicated small-animal PET scanner (Inveon Dedicated PET,
489 Preclinical Solutions, Siemens Healthcare Molecular Imaging, Knoxville, TN, USA), as
490 previously described (Brunner *et al*, 2012). Anaesthesia was induced with isoflurane (2.5%),
491 delivered via a face mask in pure oxygen at a rate of 1.2 L/min and maintained with isoflurane
492 (1.5%). Approximately 15 MBq 2-deoxy-2-[18F]fluoro-D-glucose ([18F]-FDG) (~100 µL) were
493 administered through a teil vein catheter and slowly flushed immediately afterwards with 50 µL
494 saline solution. Body temperature was monitored using a rectal thermometer and maintained
495 within the normal range using a heating pad. After placing animals within the aperture of the
496 PET scanner ECG electrodes (3M, St. Paul, MN, USA) were placed on both forepaws and the
497 left hind paw and ECG was recorded using a dedicated physiological monitoring system
498 (BioVet; Spin Systems Pty Ltd., Brisbane, Australia) (Todica *et al*, 2018). The PET emission
499 acquisition (list-mode) was initiated 30 min after [18F]-FDG injection and lasted 15 min

500 (Brunner *et al.*, 2012; Gross *et al*, 2016). For scatter and attenuation correction and additional 7-
501 min long transmission scan was performed using a Co-57 source.

502 The accuracy of the ECG trigger signal was verified retrospectively using in-house
503 software programmed in MATLAB (The Mathworks, Natick, USA) and in C programming
504 language and erroneous trigger events were removed when needed, as previously described
505 (Boning *et al*, 2013). Further processing of the data was performed using the Inveon Acquisition
506 Workplace (Siemens Medical Solutions, Knoxville, TN). As previously described, data was
507 reconstructed as a static image or as a cardiac gated image with 16 bins in a 128 × 128 matrix
508 with a zoom of 211% using an OSEM 3D algorithm with 4 and a MAP 3D algorithm with 32
509 iterations (Brunner *et al.*, 2012). The reconstructed data was normalized, corrected for randoms,
510 dead time and decay as well as attenuation and scatter.

511 PET images were analysed using the Inveon Research Workplace in a blinded manner (Siemens
512 Medical Solutions, Knoxville, TN). Infarct sizes were determined from static reconstructed
513 images using QPS® (Cedars-Sinai, Los Angeles, CA, USA). Hereby, datasets were compared to
514 a normative database and the viability defect was calculated as percentage of the left ventricular
515 volume, as described previously (Lehner *et al*, 2014; Todica *et al*, 2014). Left ventricular
516 function volumes (EDV, ESV, SV), as well as the LVEF, were determined from ECG-gated
517 images using QGS® (Cedars-Sinai, Los Angeles, CA, USA), as described previously (Brunner *et*
518 *al.*, 2012; Croteau *et al*, 2003).

519 *Statistical analysis*

520 Student's t-test or Fisher's LSD test was used (Prism GraphPad®). Welch's correction
521 for unequal variances was used when applicable. A p-value of $p < 0.05$ was considered
522 significant. Data are presented as mean +/- standard deviation (SD).

523

ACKNOLEDGEMENTS

We thank Nicole Blount, Beate Jantz, Michael Lorenz, Sebastian Helmer for excellent technical assistance.

FUNDING:

DZHK (German Centre for Cardiovascular Research) and the BMBF (German Ministry of Education and Research) (grants 81Z0600204 to CS, 81X2600252 to TW and 81X2600256 to MF). The Deutsche Forschungsgemeinschaft (SCHU 2297/1-1 and collaborative research centers 1123 project Z02 (MJ, RZ) and A07 (CS), and CRC TRR332 project A6 (CS). LMUexcellent (TW). ESC Research Grant 2021 (TW). Friedrich-Baur Stiftung (TW). Deutsche Stiftung für Herzforschung (M.F.). Chinese Scholarship Council (CSC) to JF and LL.

AUTHOR CONTRIBUTIONS:

Conceptualization: TW, CSchu

Methodology: TW, MJ, MF, JL, GP, AT, DE, CSchu

Investigation: TW, DM, MJ, MF, CG, KK, VW, SR, SA, JF, LL, WHL, JW, LT, DE, GP, SMS

Funding acquisition: TW, MF, RZ, EGP, CSchu

Supervision: AH, CW, SE, AT, RZ, CP, EGP, CSchu

Writing – original draft: TW, MJ

Writing – review & editing: all authors

Conflict of interest:

The authors declare no conflict of interest.

545 **THE PAPER EXPLAINED**

546 **Problem:** Myocardial infarction is a severe condition caused by the disruption of blood flow to
547 the heart, resulting in cell death. Inflammation plays a critical role in the myocardial infarction,
548 as it contributes to both tissue damage and reparative processes. Resident and recruited
549 macrophages are crucial immune cells involved in the inflammatory response following MI, but
550 their role in infarct healing has remained incompletely understood.

551 **Results:** By deleting a fms-intronic regulatory element (FIRE) in the Csf1r locus, we established
552 a model with chronic absence of yolk sac-derived resident macrophages, while the recruitment of
553 monocyte-derived macrophages to the infarcted heart remained intact. The absence of resident
554 macrophages resulted in altered immune cell crosstalk and proinflammatory neutrophil
555 polarization, leading to impaired cardiac remodeling after I/R injury but did not influence infarct
556 size. In contrast, abrogation of CSF1R-signaling with PLX5622 depleted both resident and
557 recruited macrophage populations, resulting in worsened cardiac remodeling and increased
558 infarct size after I/R injury.

559 **Impact:** These findings determine the distinct contributions and beneficial effects of
560 macrophage populations in myocardial infarction, and contribute to our understanding of the
561 immune response to I/R injury. This may contribute to identifying macrophage subpopulations
562 for specific pharmaceutical targeting.
563
564

565 **References**

566 Ahmad FB, Anderson RN (2021) The Leading Causes of Death in the US for 2020. *JAMA*
567 Amorim A, De Feo D, Friebel E, Ingelfinger F, Anderfuhren CD, Krishnarajah S, Andreadou M, Welsh CA, Liu Z,
568 Ginhoux F *et al* (2022) IFNgamma and GM-CSF control complementary differentiation programs in the monocyte-
569 to-phagocyte transition during neuroinflammation. *Nat Immunol* 23: 217-228
570 Armingol E, Officer A, Harismendy O, Lewis NE (2021) Deciphering cell-cell interactions and communication
571 from gene expression. *Nat Rev Genet* 22: 71-88
572 Bajpai G, Bredemeyer A, Li W, Zaitsev K, Koenig AL, Lokshina I, Mohan J, Ivey B, Hsiao HM, Weinheimer C *et*
573 *al* (2019) Tissue Resident CCR2- and CCR2+ Cardiac Macrophages Differentially Orchestrate Monocyte
574 Recruitment and Fate Specification Following Myocardial Injury. *Circ Res* 124: 263-278
575 Bajpai G, Schneider C, Wong N, Bredemeyer A, Hulsmans M, Nahrendorf M, Epelman S, Kreisel D, Liu Y, Itoh A
576 *et al* (2018) The human heart contains distinct macrophage subsets with divergent origins and functions. *Nat Med*
577 24: 1234-1245
578 Benz C, Martins VC, Radtke F, Bleul CC (2008) The stream of precursors that colonizes the thymus proceeds
579 selectively through the early T lineage precursor stage of T cell development. *J Exp Med* 205: 1187-1199
580 Blighe K RS, Lewis M, 2021. EnhancedVolcano: Publication-ready volcano plots with enhanced colouring and
581 labeling. R package version 1.10.0, https://githubcom/kevinblighe/EnhancedVolcano
582 Boning G, Todica A, Vai A, Lehner S, Xiong G, Mille E, Ilhan H, la Fougere C, Bartenstein P, Hacker M (2013)
583 Erroneous cardiac ECG-gated PET list-mode trigger events can be retrospectively identified and replaced by an
584 offline reprocessing approach: first results in rodents. *Phys Med Biol* 58: 7937-7959
585 Brunner S, Todica A, Boning G, Nekolla SG, Wildgruber M, Lehner S, Sauter M, Ubleis C, Klingel K, Cumming P
586 *et al* (2012) Left ventricular functional assessment in murine models of ischemic and dilated cardiomyopathy using
587 [18 F]FDG-PET: comparison with cardiac MRI and monitoring erythropoietin therapy. *EJNMMI Res* 2: 43
588 Buch T, Heppner FL, Tertilt C, Heinen TJ, Kremer M, Wunderlich FT, Jung S, Waisman A (2005) A Cre-inducible
589 diphtheria toxin receptor mediates cell lineage ablation after toxin administration. *Nat Methods* 2: 419-426
590 Croteau E, Benard F, Cadorette J, Gauthier ME, Aliaga A, Bentourkia M, Lecomte R (2003) Quantitative gated PET
591 for the assessment of left ventricular function in small animals. *J Nucl Med* 44: 1655-1661
592 Cuartero MI, Ballesteros I, Moraga A, Nombela F, Vivancos J, Hamilton JA, Corbi AL, Lizasoain I, Moro MA
593 (2013) N2 neutrophils, novel players in brain inflammation after stroke: modulation by the PPARgamma agonist
594 rosiglitazone. *Stroke* 44: 3498-3508
595 Dick SA, Macklin JA, Nejat S, Momen A, Clemente-Casares X, Althagafi MG, Chen J, Kantores C, Hosseinzadeh
596 S, Aronoff L *et al* (2019) Self-renewing resident cardiac macrophages limit adverse remodeling following
597 myocardial infarction. *Nat Immunol* 20: 29-39
598 Dick SA, Wong A, Hamidzada H, Nejat S, Nechanitzky R, Vohra S, Mueller B, Zaman R, Kantores C, Aronoff L *et*
599 *al* (2022) Three tissue resident macrophage subsets coexist across organs with conserved origins and life cycles. *Sci*
600 *Immunol* 7: eabf7777
601 Dimitrijevic OB, Stamatovic SM, Keep RF, Andjelkovic AV (2007) Absence of the chemokine receptor CCR2
602 protects against cerebral ischemia/reperfusion injury in mice. *Stroke* 38: 1345-1353
603 Emambokus N, Vegiopoulos A, Harman B, Jenkinson E, Anderson G, Frampton J (2003) Progression through key
604 stages of haemopoiesis is dependent on distinct threshold levels of c-Myb. *EMBO J* 22: 4478-4488
605 Epelman S, Lavine KJ, Beaudin AE, Sojka DK, Carrero JA, Calderon B, Brija T, Gautier EL, Ivanov S, Satpathy
606 AT *et al* (2014) Embryonic and adult-derived resident cardiac macrophages are maintained through distinct
607 mechanisms at steady state and during inflammation. *Immunity* 40: 91-104
608 Frieler RA, Nadimpalli S, Boland LK, Xie A, Kooistra LJ, Song J, Chung Y, Cho KW, Lumeng CN, Wang MM *et*
609 *al* (2015) Depletion of macrophages in CD11b diphtheria toxin receptor mice induces brain inflammation and
610 enhances inflammatory signaling during traumatic brain injury. *Brain Res* 1624: 103-112
611 Gerber Y, Weston SA, Enriquez-Sarano M, Berardi C, Chamberlain AM, Manemann SM, Jiang R, Dunlay SM,
612 Roger VL (2016) Mortality Associated With Heart Failure After Myocardial Infarction: A Contemporary
613 Community Perspective. *Circ Heart Fail* 9: e002460
614 Ginhoux F, Greter M, Leboeuf M, Nandi S, See P, Gokhan S, Mehler MF, Conway SJ, Ng LG, Stanley ER *et al*
615 (2010) Fate mapping analysis reveals that adult microglia derive from primitive macrophages. *Science* 330: 841-845
616 Girardot C, Scholtalbers J, Sauer S, Su SY, Furlong EE (2016) Je, a versatile suite to handle multiplexed NGS
617 libraries with unique molecular identifiers. *BMC Bioinformatics* 17: 419

618 Gomez Perdiguero E, Klapproth K, Schulz C, Busch K, Azzoni E, Crozet L, Garner H, Trouillet C, de Bruijn MF,
619 Geissmann F *et al* (2015) Tissue-resident macrophages originate from yolk-sac-derived erythro-myeloid
620 progenitors. *Nature* 518: 547-551
621 Gordon S, Martinez FO (2010) Alternative activation of macrophages: mechanism and functions. *Immunity* 32: 593-
622 604
623 Gross L, Paintmayer L, Lehner S, Brandl L, Brenner C, Grabmaier U, Huber B, Bartenstein P, Theiss HD, Franz
624 WM *et al* (2016) FDG-PET reveals improved cardiac regeneration and attenuated adverse remodelling following
625 Sitagliptin + G-CSF therapy after acute myocardial infarction. *Eur Heart J Cardiovasc Imaging* 17: 136-145
626 Guo H, Jin D, Chen X (2014) Lipocalin 2 is a regulator of macrophage polarization and NF-kappaB/STAT3
627 pathway activation. *Mol Endocrinol* 28: 1616-1628
628 Hafemeister C, Satija R (2019) Normalization and variance stabilization of single-cell RNA-seq data using
629 regularized negative binomial regression. *Genome Biol* 20: 296
630 Heidt T, Courties G, Dutta P, Sager HB, Sebas M, Iwamoto Y, Sun Y, Da Silva N, Panizzi P, van der Laan AM *et al*
631 (2014) Differential contribution of monocytes to heart macrophages in steady-state and after myocardial infarction.
632 *Circ Res* 115: 284-295
633 Hilgendorf I, Gerhardt LM, Tan TC, Winter C, Holderried TA, Chousterman BG, Iwamoto Y, Liao R, Zirlik A,
634 Scherer-Crosbie M *et al* (2014) Ly-6Chigh monocytes depend on Nr4a1 to balance both inflammatory and
635 reparative phases in the infarcted myocardium. *Circ Res* 114: 1611-1622
636 Honold L, Nahrendorf M (2018) Resident and Monocyte-Derived Macrophages in Cardiovascular Disease. *Circ Res*
637 122: 113-127
638 Hulsmans M, Clauss S, Xiao L, Aguirre AD, King KR, Hanley A, Hucker WJ, Wulfers EM, Seemann G, Courties G
639 *et al* (2017) Macrophages Facilitate Electrical Conduction in the Heart. *Cell* 169: 510-522 e520
640 Jacome-Galarza CE, Percin GI, Muller JT, Mass E, Lazarov T, Eitler J, Rauner M, Yadav VK, Crozet L, Bohm M *et*
641 *al* (2019) Developmental origin, functional maintenance and genetic rescue of osteoclasts. *Nature* 568: 541-545
642 Jin S, Guerrero-Juarez CF, Zhang L, Chang I, Ramos R, Kuan CH, Myung P, Plikus MV, Nie Q (2021) Inference
643 and analysis of cell-cell communication using CellChat. *Nat Commun* 12: 1088
644 Kubota A, Suto A, Suzuki K, Kobayashi Y, Nakajima H (2019) Matrix metalloproteinase-12 produced by
645 Ly6C(low) macrophages prolongs the survival after myocardial infarction by preventing neutrophil influx. *J Mol*
646 *Cell Cardiol* 131: 41-52
647 Kuhn R, Schwenk F, Aguet M, Rajewsky K (1995) Inducible gene targeting in mice. *Science* 269: 1427-1429
648 Lehner S, Todica A, Vanchev Y, Uebleis C, Wang H, Herrler T, Wangler C, Cumming P, Boning G, Franz WM *et*
649 *al* (2014) In vivo monitoring of parathyroid hormone treatment after myocardial infarction in mice with
650 [68Ga]annexin A5 and [18F]fluorodeoxyglucose positron emission tomography. *Mol Imaging* 13: 1-8
651 Liao Y, Smyth GK, Shi W (2014) featureCounts: an efficient general purpose program for assigning sequence reads
652 to genomic features. *Bioinformatics* 30: 923-930
653 Love MI, Huber W, Anders S (2014) Moderated estimation of fold change and dispersion for RNA-seq data with
654 DESeq2. *Genome Biol* 15: 550
655 Lozano R, Naghavi M, Foreman K, Lim S, Shibuya K, Aboyans V, Abraham J, Adair T, Aggarwal R, Ahn SY *et al*
656 (2012) Global and regional mortality from 235 causes of death for 20 age groups in 1990 and 2010: a systematic
657 analysis for the Global Burden of Disease Study 2010. *Lancet* 380: 2095-2128
658 Mass E, Ballesteros I, Farlik M, Halbritter F, Gunther P, Crozet L, Jacome-Galarza CE, Handler K, Klughammer J,
659 Kobayashi Y *et al* (2016) Specification of tissue-resident macrophages during organogenesis. *Science* 353
660 McInnes L, Healy J, Melville J (2020) UMAP: Uniform Manifold Approximation and Projection for Dimension
661 Reduction. *arXiv*
662 McInnes L, Healy J, Saul N, Großberger L (2018) UMAP: Uniform Manifold Approximation and Projection. *J*
663 *Open Source Softw* 3, (29), 861
664 Munro DAD, Bradford BM, Mariani SA, Hampton DW, Vink CS, Chandran S, Hume DA, Pridans C, Priller J
665 (2020) CNS macrophages differentially rely on an intronic Csf1r enhancer for their development. *Development* 147
666 Muzumdar MD, Tasic B, Miyamichi K, Li L, Luo L (2007) A global double-fluorescent Cre reporter mouse.
667 *Genesis* 45: 593-605
668 Nahrendorf M, Swirski FK, Aikawa E, Stangenberg L, Wurdinger T, Fig ueiredo JL, Libby P, Weissleder R, Pittet
669 MJ (2007) The healing myocardium sequentially mobilizes two monocyte subsets with divergent and
670 complementary functions. *J Exp Med* 204: 3037-3047
671 Nicolas-Avila JA, Lechuga-Vieco AV, Esteban-Martinez L, Sanchez-Diaz M, Diaz-Garcia E, Santiago DJ, Rubio-
672 Ponce A, Li JL, Balachander A, Quintana JA *et al* (2020) A Network of Macrophages Supports Mitochondrial
673 Homeostasis in the Heart. *Cell* 183: 94-109 e123

674 Oh DS, Oh JE, Jung HE, Lee HK (2017) Transient Depletion of CD169(+) Cells Contributes to Impaired Early
675 Protection and Effector CD8(+) T Cell Recruitment against Mucosal Respiratory Syncytial Virus Infection. *Front*
676 *Immunol* 8: 819
677 Panizzi P, Swirski FK, Fig ueiredo JL, Waterman P, Sosnovik DE, Aikawa E, Libby P, Pittet M, Weissleder R,
678 Nahrendorf M (2010) Impaired infarct healing in atherosclerotic mice with Ly-6C(hi) monocytosis. *J Am Coll*
679 *Cardiol* 55: 1629-1638
680 Parmar T, Parmar VM, Perusek L, Georges A, Takahashi M, Crabb JW, Maeda A (2018) Lipocalin 2 Plays an
681 Important Role in Regulating Inflammation in Retinal Degeneration. *J Immunol* 200: 3128-3141
682 Peng H, Long F, Ding C (2005) Feature selection based on mutual information: criteria of max-dependency, max-
683 relevance, and min-redundancy. *IEEE Trans Pattern Anal Mach Intell* 27: 1226-1238
684 Percin GI, Eitler J, Kranz A, Fu J, Pollard JW, Naumann R, Waskow C (2018) CSF1R regulates the dendritic cell
685 pool size in adult mice via embryo-derived tissue-resident macrophages. *Nat Commun* 9: 5279
686 Revelo X, Parthiban P, Chen C, Barrow F, Fredrickson G, Wang H, Yucel D, Herman A, van Berlo JH (2021)
687 Cardiac Resident Macrophages Prevent Fibrosis and Stimulate Angiogenesis. *Circ Res*
688 Rojo R, Raper A, Ozdemir DD, Lefevre L, Grabert K, Wollscheid-Lengeling E, Bradford B, Caruso M, Gazova I,
689 Sanchez A *et al* (2019) Deletion of a Csf1r enhancer selectively impacts CSF1R expression and development of
690 tissue macrophage populations. *Nat Commun* 10: 3215
691 Ruedl C, Jung S (2018) DTR-mediated conditional cell ablation-Progress and challenges. *Eur J Immunol* 48: 1114-
692 1119
693 Sager HB, Hulsmans M, Lavine KJ, Moreira MB, Heidt T, Courties G, Sun Y, Iwamoto Y, Tricot B, Khan OF *et al*
694 (2016) Proliferation and Recruitment Contribute to Myocardial Macrophage Expansion in Chronic Heart Failure.
695 *Circ Res* 119: 853-864
696 Schulz C, Gomez Perdiguero E, Chorro L, Szabo-Rogers H, Cagnard N, Kierdorf K, Prinz M, Wu B, Jacobsen SE,
697 Pollard JW *et al* (2012) A lineage of myeloid cells independent of Myb and hematopoietic stem cells. *Science* 336:
698 86-90
699 Sivakumaran S, Henderson S, Ward S, Sousa PS, Manzo T, Zhang L, Conlan T, Means TK, D'Aveni M, Hermine O
700 *et al* (2016) Depletion of CD11c(+) cells in the CD11c.DTR model drives expansion of unique CD64(+) Ly6C(+)
701 monocytes that are poised to release TNF-alpha. *Eur J Immunol* 46: 192-203
702 Srinivas S, Watanabe T, Lin CS, William CM, Tanabe Y, Jessell TM, Costantini F (2001) Cre reporter strains
703 produced by targeted insertion of EYFP and ECFP into the ROSA26 locus. *BMC Dev Biol* 1: 4
704 Stremmel C, Schuchert R, Schneider V, Weinberger T, Thaler R, Messerer D, Helmer S, Geissmann F, Frampton J,
705 Massberg S *et al* (2018) Inducible disruption of the c-myb gene allows allogeneic bone marrow transplantation
706 without irradiation. *J Immunol Methods* 457: 66-72
707 Stuart T, Satija R (2019) Integrative single-cell analysis. *Nat Rev Genet* 20: 257-272
708 Talbot J, Bianchini FJ, Nascimento DC, Oliveira RD, Souto FO, Pinto LG, Peres RS, Silva JR, Almeida SC,
709 Louzada-Junior P *et al* (2015) CCR2 Expression in Neutrophils Plays a Critical Role in Their Migration Into the
710 Joints in Rheumatoid Arthritis. *Arthritis Rheumatol* 67: 1751-1759
711 Todica A, Beetz NL, Gunther L, Zacherl MJ, Grabmaier U, Huber B, Bartenstein P, Brunner S, Lehner S (2018)
712 Monitoring of Cardiac Remodeling in a Mouse Model of Pressure-Overload Left Ventricular Hypertrophy with
713 [(18)F]FDG MicroPET. *Mol Imaging Biol* 20: 268-274
714 Todica A, Zacherl MJ, Wang H, Boning G, Jansen NL, Wangler C, Bartenstein P, Kreissl MC, Hacker M, Brunner
715 S *et al* (2014) In-vivo monitoring of erythropoietin treatment after myocardial infarction in mice with
716 [(6)(8)Ga]Annexin A5 and [(1)(8)F]FDG PET. *J Nucl Cardiol* 21: 1191-1199
717 Weinberger T, Esfandyari D, Messerer D, Percin G, Schleifer C, Thaler R, Liu L, Stremmel C, Schneider V,
718 Vagnozzi RJ *et al* (2020) Ontogeny of arterial macrophages defines their functions in homeostasis and
719 inflammation. *Nat Commun* 11: 4549
720 Weinberger T, Schulz C (2015) Myocardial infarction: a critical role of macrophages in cardiac remodeling. *Front*
721 *Physiol* 6: 107
722 Xu P, Zhang J, Wang H, Wang G, Wang CY, Zhang J (2017) CCR2 dependent neutrophil activation and
723 mobilization rely on TLR4-p38 axis during liver ischemia-reperfusion injury. *Am J Transl Res* 9: 2878-2890
724 Yates AD, Achuthan P, Akanni W, Allen J, Allen J, Alvarez-Jarreta J, Amode MR, Armean IM, Azov AG, Bennett
725 R *et al* (2020) Ensembl 2020. *Nucleic Acids Res* 48: D682-D688
726 Zaman R, Epelman S (2022) Resident cardiac macrophages: Heterogeneity and function in health and disease.
727 *Immunity* 55: 1549-1563
728

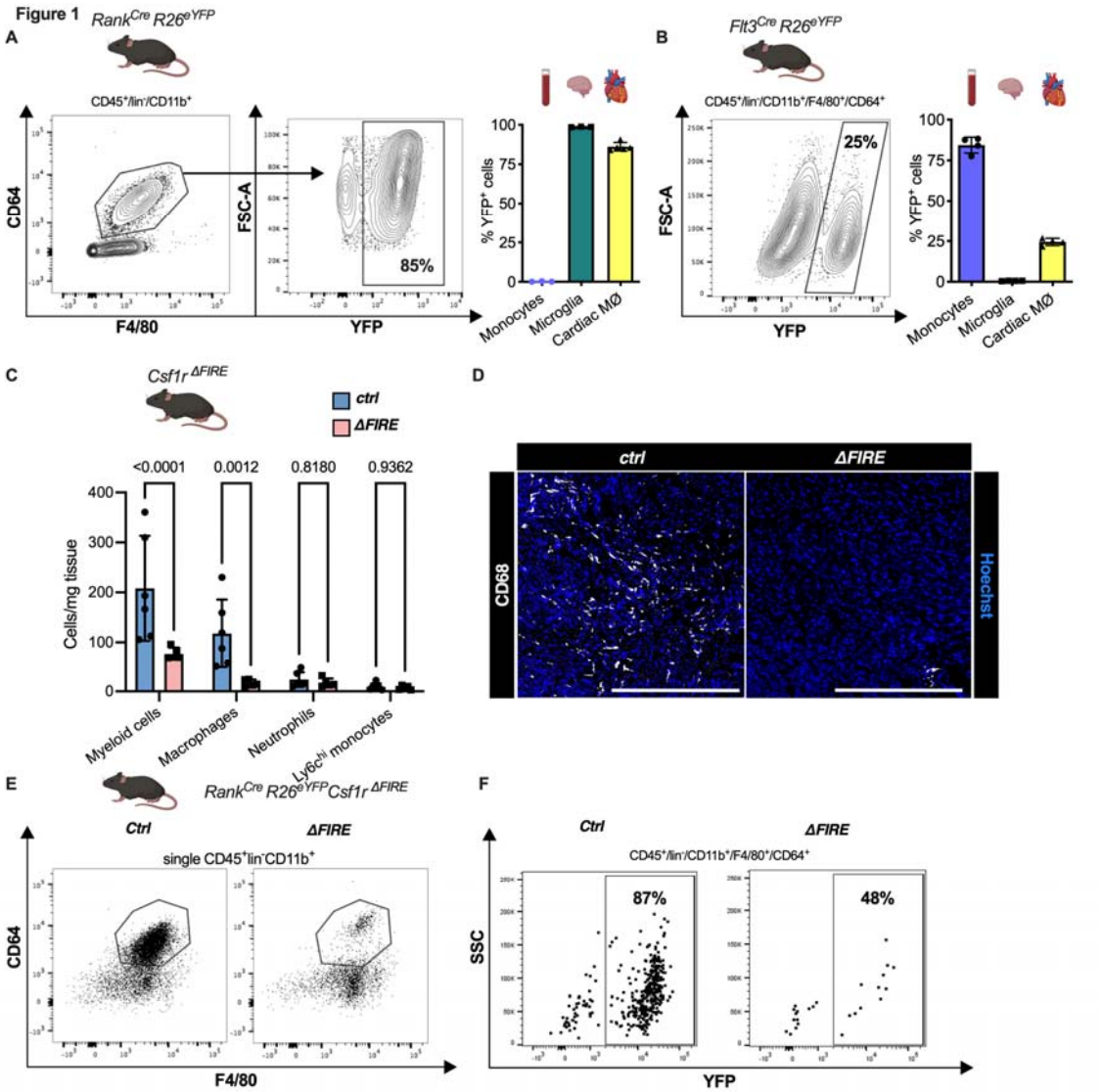

Figure 1. Absence of resident cardiac macrophages in *Csf1r*$^{\Delta FIRE}$ mice.
(A) Flow cytometry analysis of 3 month-old *Rank*^{Cre}*Rosa26*^{eYFP} mice, showing single/CD45^{+}/lin- (CD11c, Ter119, Tcrß, Nk1.1)/CD11b^{+} cardiac cells, eYFP expression in macrophages (CD64^{+}/F4/80^{+}) and percentage of eYFP^{+} blood monocytes, microglia and cardiac macrophages (n=3-5 each from an independent experiment). (B) Flow cytometry analysis of 3 month-old *Flt3*^{Cre}*Rosa26*^{eYFP} mice, showing macrophage expression of eYFP and percentage of eYFP^{+} blood monocytes, microglia and cardiac macrophages (n=4 each from an independent experiment). **(C)** Number of myeloid cells (CD45^{+}/lin^{-}/CD11b^{+}), macrophages (CD45^{+}/lin^{-}/CD11b^{+}/CD64^{+}/F4/80^{+}), neutrophils (CD45^{+}/lin^{-}/CD11b^{+}/CD64^{-}/F4/80^{-}/Ly6g^{+}) and Ly6c^{hi} monocytes (CD45^{+}/lin^{-}/CD11b^{+}/CD64^{-}/F4/80^{-}/Ly6g-/Ly6c^{hi}) (*n=6 for control* and n=5 for Δ*FIRE* mice, each single experiments). **(D)** Representative immunohistological images showing macrophages (CD68^{+} cells in white and Hoechst in blue) in *control* and Δ*FIRE* hearts in 3 month-old mice at baseline conditions (scale bars represent 500µm). **(E)** Representative flow cytometry analysis of cardiac macrophages and **(F)** their expression of eYFP in *Csf1r*$^{\Delta FIRE/+}$*Rank*^{Cre}*Rosa26*^{eYFP} *and Csf1r*$^{\Delta FIRE/\Delta FIRE}$*Rank*^{Cre}*Rosa26*^{eYFP}. Either Fisher's LSD test or unpaired t-test were performed and mean ± SD is shown.

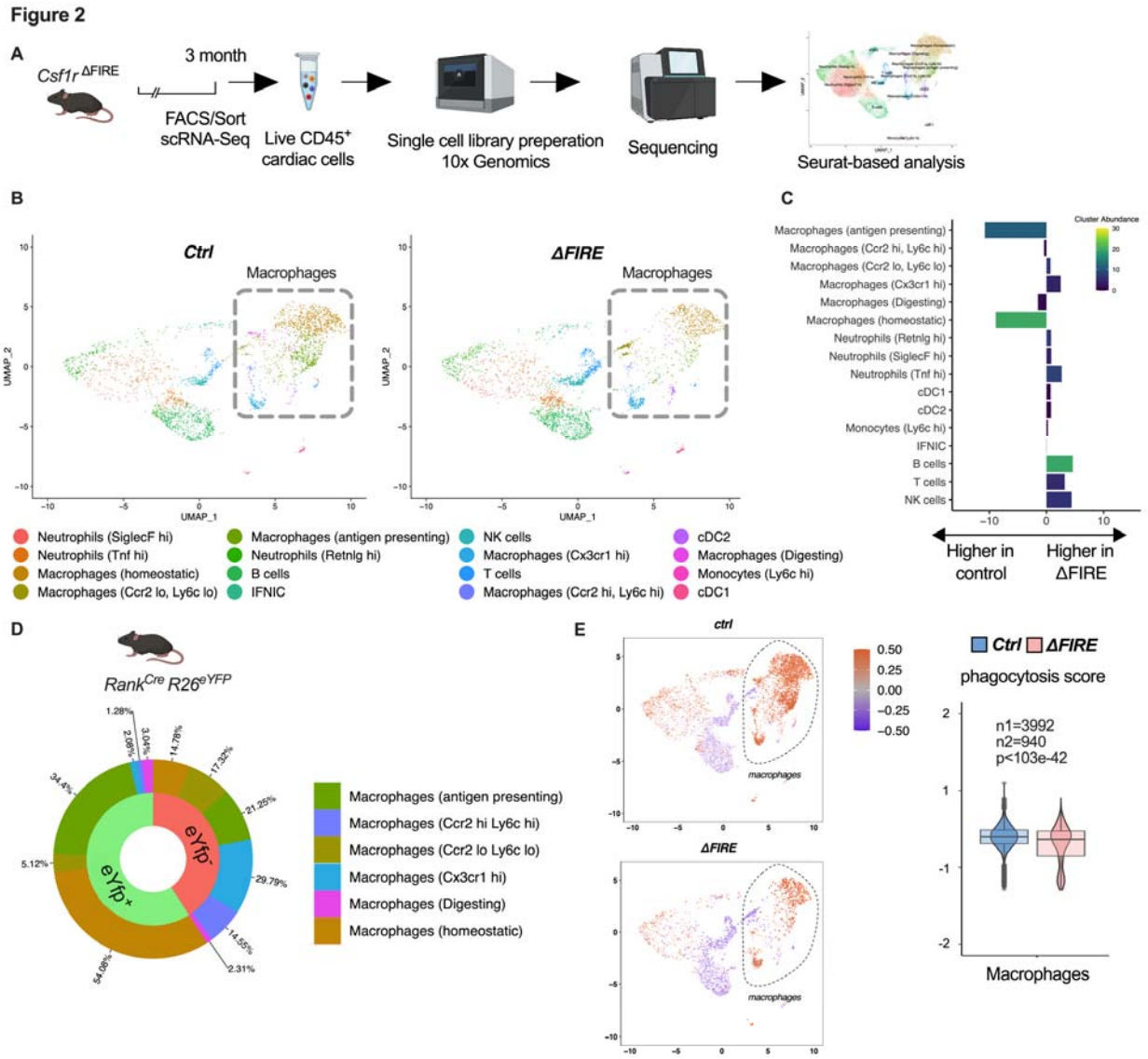

Figure 2. Changes in the cardiac immune phenotype in *Csf1r$^{\Delta FIRE}$* mice in baseline conditions.

(A) Experimental setup to analyze cardiac immune cells using scRNA-seq of sorted CD45^{+}/live cells. **(B)** UMAPs of control and ΔFIRE in baseline conditions (n=3 for *control* and Δ*FIRE)* **(C)** Absolute difference (percentage points) in cluster abundance between *control* and Δ*FIRE*. **(D)** Contribution of EMP-derived (*eYfp* expressing) macrophages to the different macrophage clusters analysed by scRNA-seq analysis of immune cells harvested from a *Rank^{Cre}Rosa26^{eYFP}* mouse. **(E)** Phagocytosis score projected on a UMAP displaying *control and* Δ*FIRE* immune cell subsets. Violin and box plots show the computed phagocytosis score combined in all macrophage clusters (n1/n2 represents number of cells from control/ Δ*FIRE* mice).

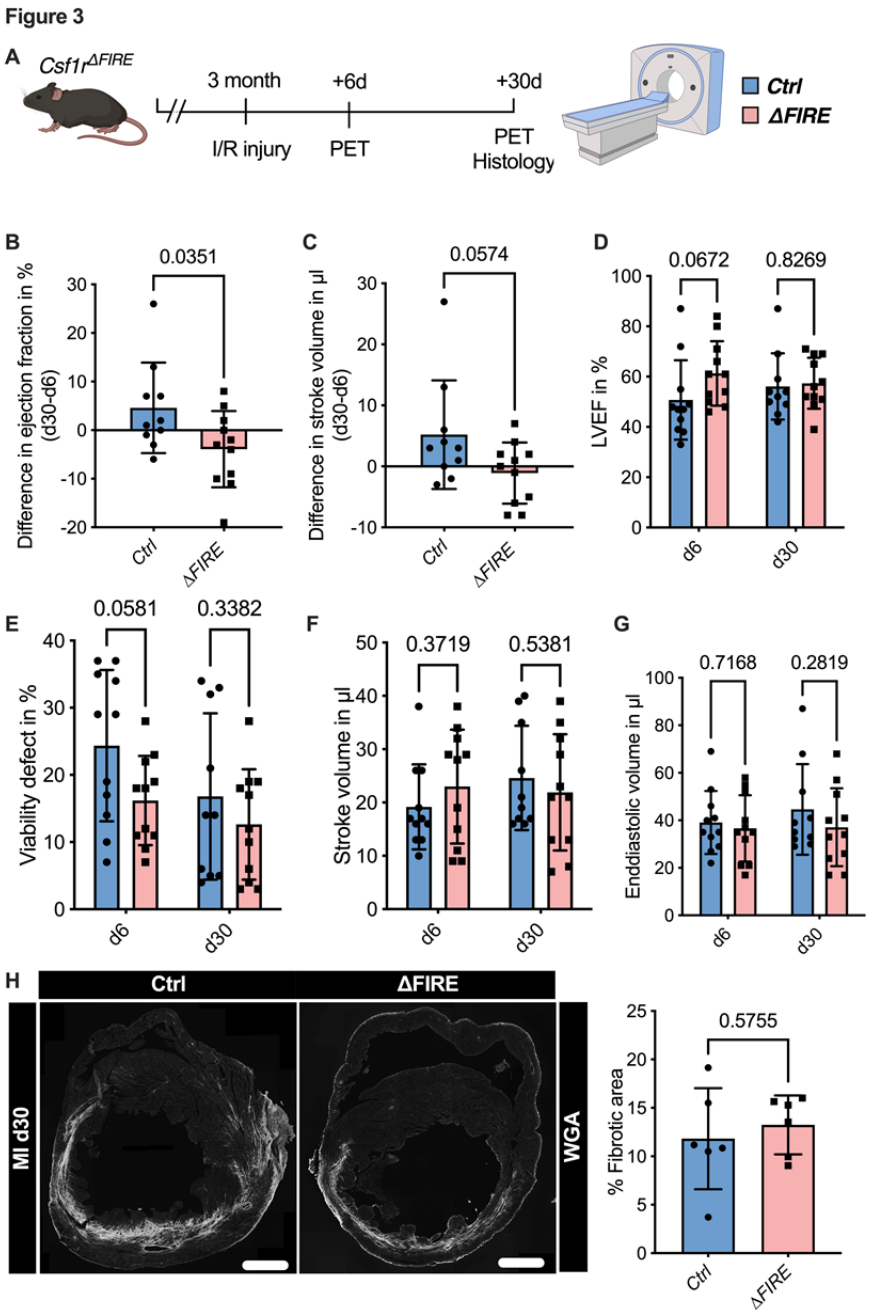

Figure 3. Adverse cardiac remodeling in *Csf1r*$^{\Delta FIRE}$ mice after I/R injury

(A) Schematic of the sequential analysis of cardiac function, dimensions and viability using positron-emission tomography 6 and 30 days after I/R injury in *control* and Δ*FIRE* with (B and C) showing the intraindividual changes in each parameter from d6 to d30 and (D-G) the individual timepoints on d6 and d30 (d6: n=11 for *control and* Δ*FIRE*, d30: n=10 for *control and n=11 for* Δ*FIRE*). **(B and D)** left ventricular ejection fraction (LVEF), **(C and E)** percentage of the viability defect, **(F)** stroke volume and **(F)** left-ventricular end-diastolic volume**.** **(H)** Representative immunohistological images showing the fibrotic area (WGA^{+} area) in hearts from *control and ΔFIRE* mice 30 days after I/R injury. Right panel shows the percentage of fibrotic

area in the respective groups (n= 6 for each group). Student's t-test was performed and mean ± SD is shown.

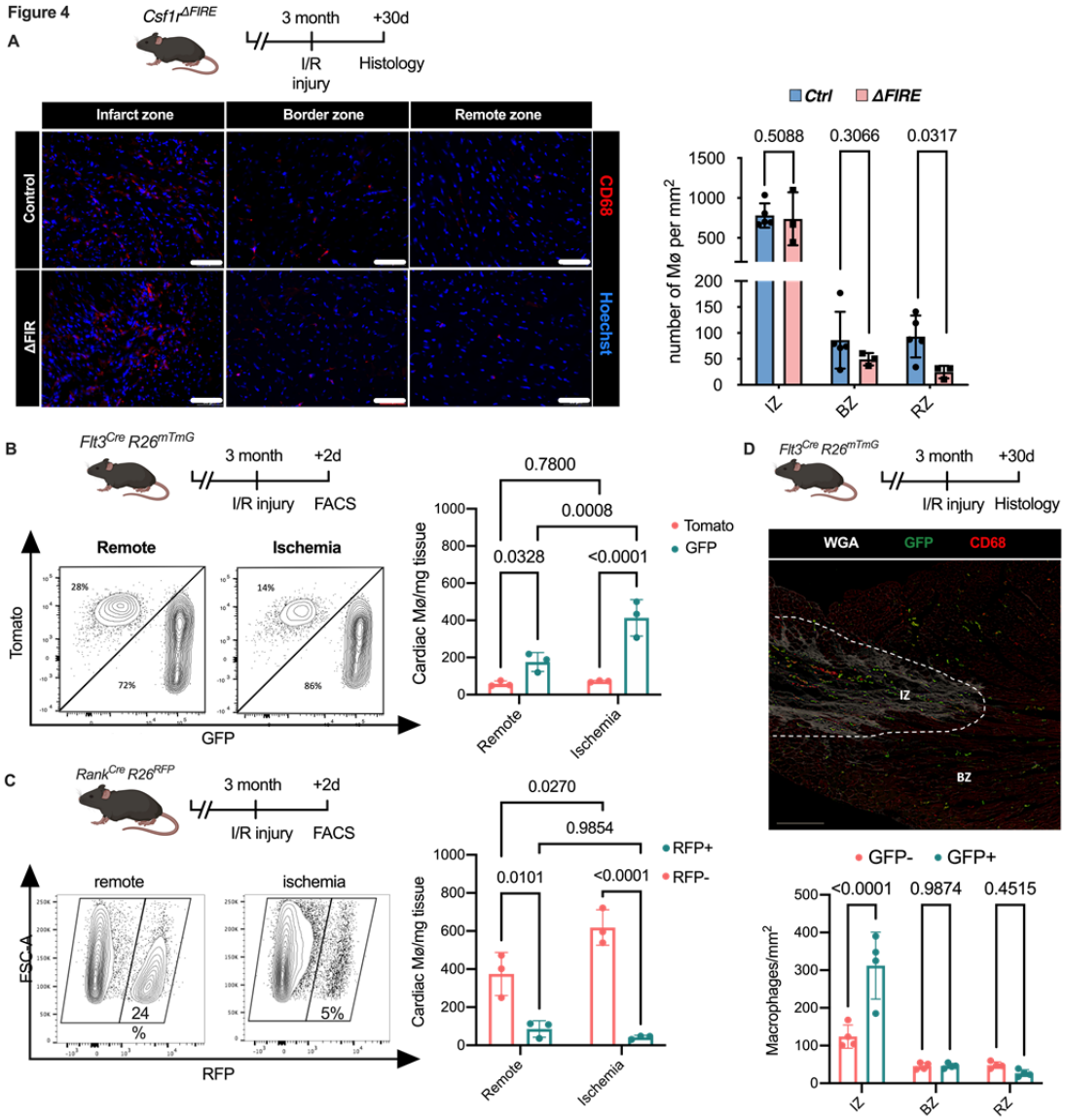

Figure 4. Recruitment of BM-derived macrophages into infarct zone of *Csf1r*$^{\Delta FIRE}$ mice. **(A)** Representative immunohistology of hearts from Δ*FIRE* mice 30 days after I/R injury showing macrophages (CD68^{+} cells in red and Hoechst in blue) in the infarct, border and remote zone. Right panel shows number of cardiac macrophages in the respective area (n=5 *control* and n=3 for Δ*FIRE*). **(B)** Flow cytometry analysis of *Flt3*^{Cre}*Rosa26*$^{mT/mG}$ mice 2 days after I/R injury, (left) representative flow cytometry showing expression of tomato and GFP in macrophages in the remote and ischemic myocardium and (right) number of tomato^{+} and GFP^{+} cardiac macrophages in the respective area (n=3, each individual experiments). **(C)** Flow cytometry analysis of *Rank*^{Cre}*Rosa26*^{RFP} mice 2 days after I/R injury, (left) representative flow cytometry showing expression of RFP in macrophages in the remote and ischemic myocardium and (right) number of RFP^{-} and RFP^{+} cardiac macrophages in the respective area (n=3, each individual experiments). **(D)** Histological analysis of *Flt3*^{Cre}*Rosa26*$^{mT/mG}$ mice 30 days after I/R injury in the infarct, border and remote zone, (left) representative immunohistology of the infarct and border

zone and (right) number of GFP$^-$ and GFP$^+$ cardiac macrophages in the respective areas (n=4). Fishers LSD test was performed for all experiments and mean ± SD is shown.

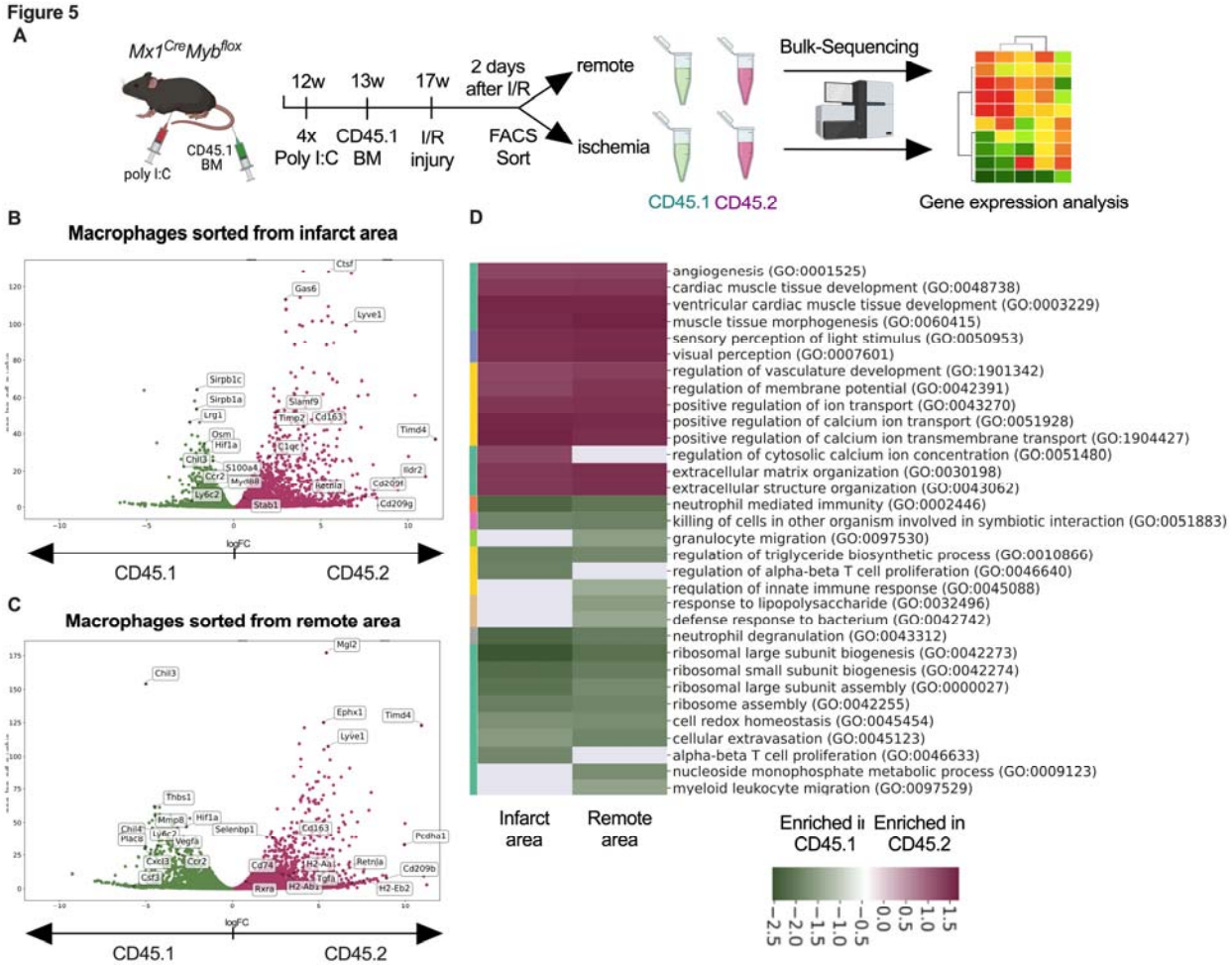

Figure 5. Transcriptional landscape of resident versus recruited macrophages in I/R injury **(A)** Experimental setup to generate non-irradiation BM chimera using *CD45.2 Mx1^{Cre}Myb$^{flox/flox}$* and transplantation of CD45.1 BM. I/R injury was induced 4 weeks after BM-transplantation and CD45.1$^+$ and CD45.2$^+$ macrophages were sorted from the remote and ischemic myocardium 2 days after I/R injury and RNA-sequencing was performed on bulk cells**. (B and C)** Volcano plot showing differential gene expression analysis results of recruited CD45.1 vs. resident CD45.2 macrophages in the **(B)** remote and **(C)** ischemic zone. **(D)** Gene ontology enrichment analysis showing specific biological processes enriched in CD45.1 and CD45.2 macrophages in the ischemic and remote zone.

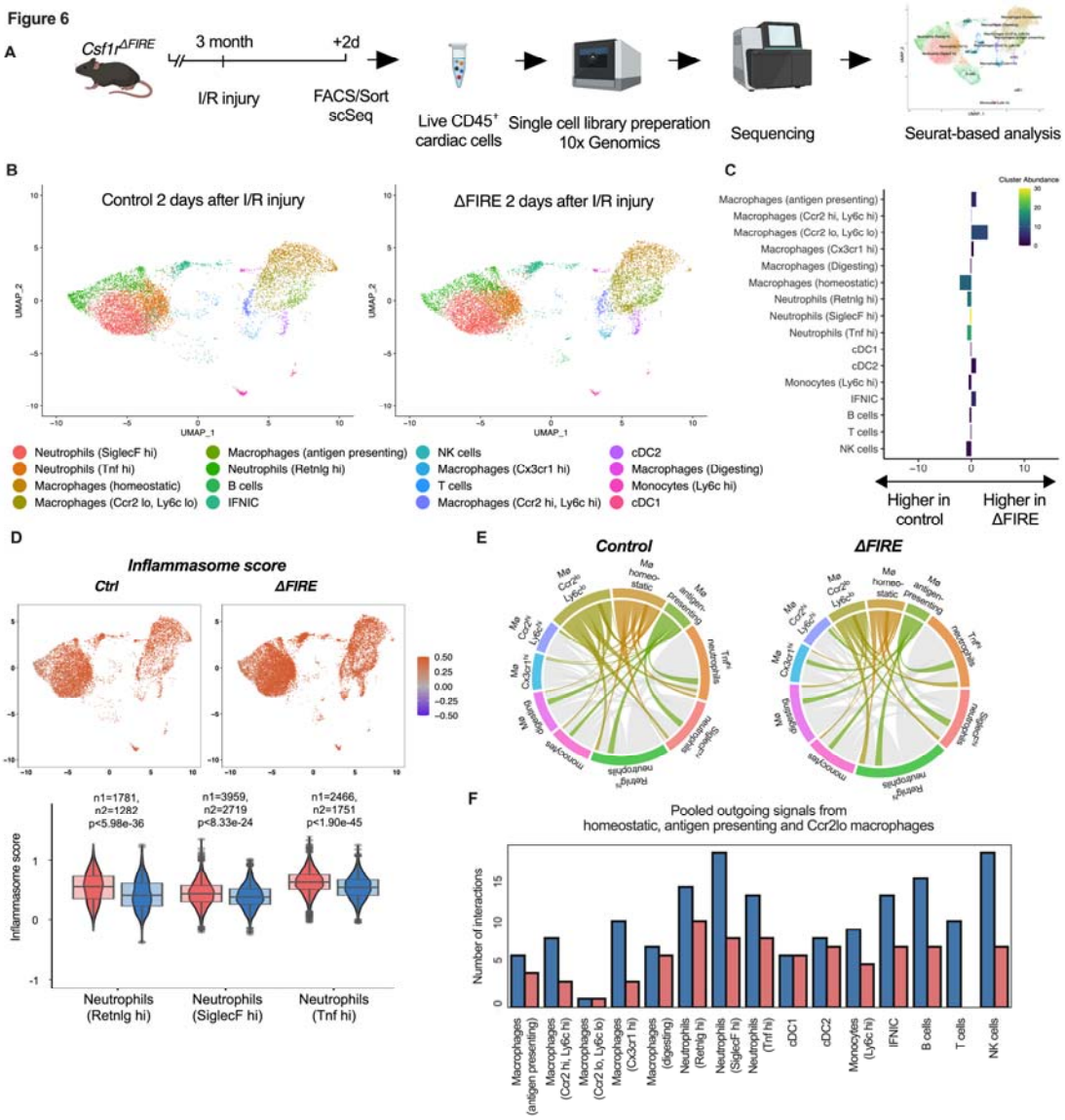

Figure 6. **Altered inflammatory patterns and immune cell communication in *Csf1r*$^{\Delta FIRE}$ mice.**

(A) Experimental setup to analyze transcriptional changes in cardiac immune cells on a single cell level 2 days after I/R injury in *ΔFIRE* mice. **(B)** UMAPs of control and ΔFIRE 2 days after I/R injury (n=2 for *control* and Δ*FIRE)*. **(C)** Absolute difference (percentage points) in cluster abundance between *control* and Δ*FIRE*. **(D)** Inflammasome score projected on a UMAP displaying control and ΔFIRE immune cell subsets after I/R injury. Violin and box plots show the computed inflammasome score in neutrophil clusters (n1/n2 represents number of cells from control/ Δ*FIRE* mice). (**E**) Ligand–receptor interactions of *antigen-presenting, Ccr2*^{lo} *ly6c*^{lo} *and homeostatic macrophages* (highlighted) with other immune cell clusters. Shown are the aggregated communication scores (width of interactions) for all cell types. Only communication scores larger than 6 are considered. (**F**) Number of interactions (with communication score > 6) outgoing from homeostatic, antigen presenting and Ccr2^{lo} macrophages to other immune cell clusters.

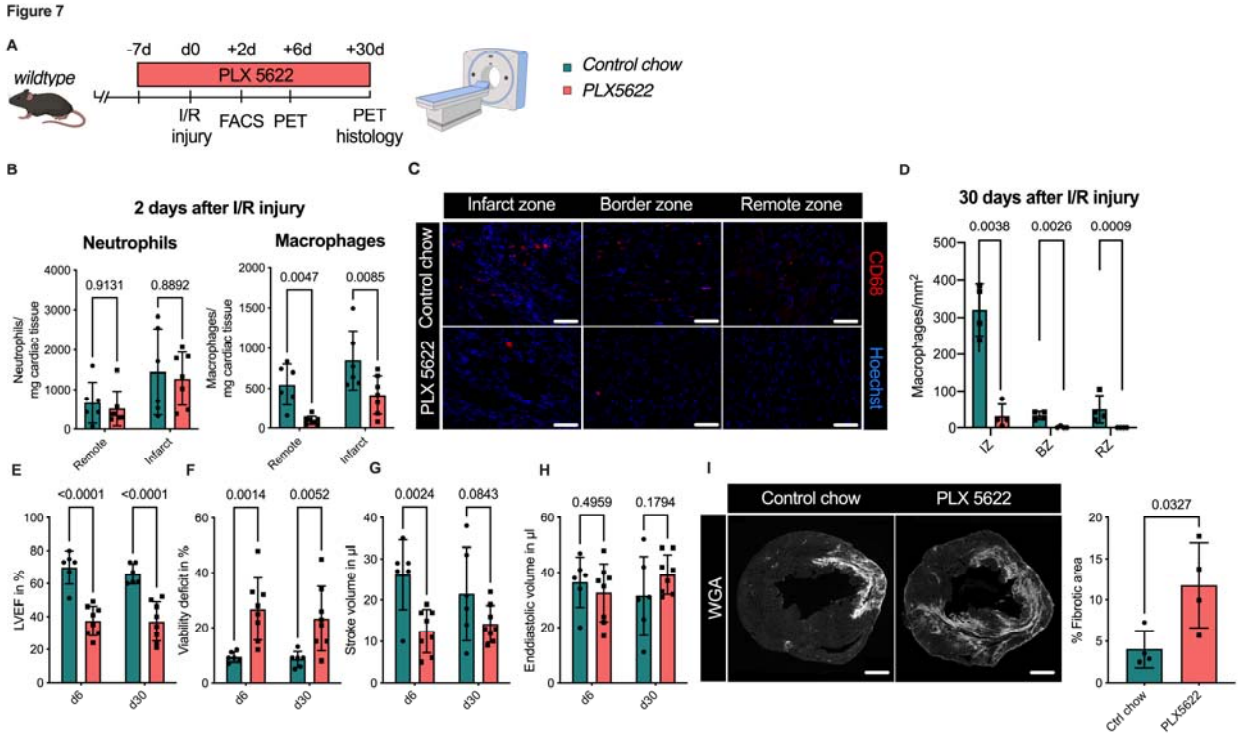

Figure 7. **Ablation of resident and recruited macrophages severely impacts on cardiac healing after I/R injury**

(**A**) Schematic of the analysis of cardiac function and infarct size in mice treated with PLX5622 7 days prior and 30 days after I/R injury. **(B)** Number of cardiac macrophages and neutrophils in the remote and ischemic myocardium 2 days after I/R injury in mice fed control chow (n=6) or PLX5622 (n=7). **(C)** Representative immunohistology of hearts 30 days after I/R injury showing macrophages ($CD68^+$ cells in red and Hoechst in blue) in the infarct, border and remote zone and **(D)** number of cardiac macrophages in the respective area (n=4 for control chow and n=4 for PLX5622). **(E)** Left ventricular ejection fraction (LVEF), **(F)** viability deficit, **(G)** stroke volume and **(H)** end-diastolic volume measured using positron-emission tomography 6 and 30 days after I/R injury (n=6 for control chow, n=8 for PLX5622). **(I)** Representative immunohistological images showing the fibrotic area (WGA^+ area) in hearts 30 days after I/R injury from mice fed control chow or PLX5622. Percentage of fibrotic area in the respective groups (n= 4 for each group). Student's t-test or Fishers LSD test was performed and mean ± SD is shown.